Du, X.; Lei, X.; Zhou, L.; Peng, Y.; Zeng, Y.; Yang, H.; Li, D.... (2022). Bimetallic Ni and Mo Nitride as an Efficient Catalyst for Hydrodeoxygenation of Palmitic Acid. ACS Catalysis. 12(8):4333-4343. https://doi.org/10.1021/acscatal.1c05847

Bimetallic Ni and Mo nitride as efficient catalyst for hydrodeoxygenation of palmitic acid

Xiangze Du [a,b], *Xiaomei Lei* [a], *Linyuan Zhou* [a], *Yong Peng* [b], *Yan Zeng* [a], *Huiru Yang* [a], *Dan Li* [a], *Changwei Hu* [a]*, *and Hermenegildo Garcia* [b]*

[a] Key Laboratory of Green Chemistry and Technology, College of Chemistry, Sichuan University, 29 Wangjiang Road, Chengdu, 610064, China.

[b] Instituto Universitario de Tecnología Química, Consejo Superior de Investigaciones Científicas.-Universitat Politecnica de Valencia, Universitat Politecnica de Valencia, Av. De los Naranjos s/n, 46022 Valencia, Spain.

E-mail: changweihu@scu.edu.cn, hgarcia@qim.upv.es

Keywords: reductive decomposition, Ni_3Mo_3N, hydrodeoxygenation, palmitic acid, bifunctional catalyst, alkanes

Abstract: In the context of the preparation of liquid fuels derived from biomass with zero CO_2 footprint, fatty acids appear as suitable feedstocks. However, reduction of carboxylic acid groups usually requires harsh reaction conditions and the development of efficient solid catalysts. Herein, bimetallic Ni-Mo nitrides have been obtained by a procedure not involving nitridation of the corresponding oxide, but reductive decomposition of the tris(ethylenediamine)nickel molybdate at temperatures between 550 and 700 ºC. Successful formation of the Ni_3Mo_3N nitride is confirmed by XRD. Ni_3Mo_3N samples are found efficient catalysts for the hydrodeoxygenation of palmitic acid to C_{15}/C_{16} alkanes with a combined

selectivity over 90 % and 100 % palmitic conversion and higher activity than analogous Ni, Mo nitride obtained by NH_3 nitridation of $NiMoO_4$. Ni_3Mo_3N is found recyclable with only a slight decay in catalytic activity upon consecutive reuses attributable to the neutralization of acid sites. The present results show the opportunity that bimetallic nitrides offer as robust advanced solid catalysts for reactions of biomass conversion requiring harsh conditions.

1. Introduction

Hydrodeoxygenation of fatty acids of the appropriate chain length is a useful reaction that can provide synthetic fuels from biomass with low CO_2-footprint.[1-3] However, in order to reach high conversions, the process requires high temperature and pressures and frequently alcohol is the final product.[4-6] Typical catalysts for long-chain carboxylic acid hydrogenation are noble or semi noble metals, including Pt, Pd, Ir, Re and Ru.[4-7] Due to the on-going shift from fossil fuels to renewable, CO_2-neutral fuels, there is a continuous interest in developing advanced catalysts for biomass conversion.[8] These catalysts should be based on abundant, first-row transition metals exhibiting high activity and selectivity that could operate under more amenable reaction conditions. Several studies in the literature have reported the catalytic activity of Ni nanoparticles on acid and basic supports for fatty acid hydrogenation.[9-11] The list includes Ni deposited on mixed Zn-Al oxide,[10] zeolites of various pore sizes and acid properties among others.[12] The catalytic hydrodeoxygenation of fatty acids promoted by Ni catalysts exhibits a synergistic effect with acidity or basicity of the support.[10, 13] Alloying of Ni with other metals, such as Pd, is also an established strategy to increase the catalytic activity of the Ni-based catalysts.[14, 15]

On the other hand, transition metal nitrides have recently attracted much attention in heterogeneous catalysis because they combine a high structural stability and thermal

conductivity with a superior activity and selectivity for several demanding reactions.[16, 17] Particularly, Mo-based nitrides have been reported to exhibit an outstanding catalytic performance for many reactions including the Fischer-Tropsch process,[18] ammonia synthesis,[19] hydrogen evolution reaction,[20] and hydrogenation reaction.[21] In this context, it is a general observation that bimetallic materials can exhibit an improved performance with respect to the corresponding monometallic analogs due to the fine tuning of electron density at the active sites that can be achieved for the optimal composition.[22, 23] In the present case, modification of Mo electron density by a second metal on the molybdenum nitride could downshift the d-band center of Mo atoms relative to Fermi level and could result in a further promotion of the catalytic activity.[24]

Taking into account the general performance of Ni for hydrodeoxygenation of fatty acids and hydrogen activation in general,[25, 26] the combination of nickel and molybdenum in a bimetallic nitride could result in a material with an interesting catalytic activity for demanding fatty acid hydrodeoxygenation reaction. On one hand, Mo nitride will provide robustness and structural stability, while Ni will introduce active hydrogenation sites. Herein, the activity as hydrodeoxygenation catalyst of fatty acids of bimetallic Ni-Mo nitrides is reported. The Ni_3Mo_3N samples prepared here are obtained by a new synthetic method that does not start from the corresponding mixed Ni-Mo oxide and has allowed us a certain control on the properties of the mixed Ni-Mo nitride, resulting in an optimization of the catalytic performance.

2. Experimental Section/Methods

Material: Ammonium molybdate tetrahydrate ($(NH_4)_6Mo_7O_{24}\cdot 4H_2O$, ≥ 99.0%), nickel(II) nitrate hexahydrate ($Ni(NO_3)_2\cdot 6H_2O$, ≥ 99.0%), and ethylenediamine ($C_2H_8N_2$, ≥ 99.0%) were

purchased from Chengdu Chron Chemical Co.. Nickel oxalate dihydrate ($NiC_2O_4 \cdot 2H_2O$, 99%) was obtained from Aladdin. All the reagents were analytically pure and used without further purification. H_2 were purchased from Southwest Chemical Research Institute Co..

Preparation of $[Ni(en)_3][MoO_4]$: The precursor of $[Ni(en)_3][MoO_4]$ was prepared using hydrothermal method. The molar ratio of $(NH_4)_6Mo_7O_{24} \cdot 4H_2O$: $NiC_2O_4 \cdot 2H_2O$: $C_2H_8N_2$: H_2O was 1:1:27.8:166.6. Typically, ammonium molybdate tetrahydrate (24.7 g), nickel oxalate dihydrate (3.7 g), ethylenediamine (33.4 g) and deionized water (60.0 g) were added into a Teflon autoclave (200 mL). The mixture was heated to 130 ºC in an oven and kept for 8 h. Then it was cooled down to room temperature at a rate of 10 ºC h^{-1}. After standing overnight, the sample was filtered and washed several times with deionized water. The obtained purple precursor was dried and stored in a desiccator for later use. XRD pattern of precursor showed diffraction peaks at 11.0 º, 17.7 º, 19.1 º, 20.9 º, 22.2 º, 23.9 º, 26.3 º and 38.2 º, which were attributed to $[Ni(en)_3][MoO_4]$. In addition, there were several unknown peaks at 28.5 º, 30.8 º, 33.5 º, 34.6 º and 38.9 º with weak diffraction intensity. In general, the result indicated that $[Ni(en)_3][MoO_4]$ was prepared successfully.

Preparation of Mo_2N and bimetallic nitride: The purple powder was pressed and ground into particles with size of 40-60 meshes. Then the sample was put into stainless steel tube and reduced under H_2 flow (40 mL min^{-1}). The heating program was from room temperature to target temperature (550 ºC, 600 ºC and 700 ºC) at a rate of 2 ºC min^{-1} and kept for 2 h. After reduction, the sample was cooled to room temperature at H_2 atmosphere. Finally, the catalyst was obtained after passivating for 10 h at a 5% O_2/He (10 mL min^{-1}) flow. Monometallic Mo_2N was prepared by nitridation of MoO_3 from room temperature to 700 ºC at a rate of 2 ºC min^{-1} and kept for 2 h under NH_3. For the bimetallic nitride synthesized from nitridation of oxide, $NiMoO_4$ was synthesized by $NiCl_2$ and $NaMoO_4 \cdot 2H_2O$ firstly, and then nitrided from

room temperature to 600 ºC at a rate of 2 ºC min^{-1} and kept for 2 h under NH_3. The prepared catalyst was placed in a desiccator for its later use.

Preparation of Ni/Al_2O_3: Ni/Al_2O_3 with 5% Ni loading was prepared by an incipient wetness impregnation method with appropriate amount of $Ni(NO_3)_2 \cdot 6H_2O$ solution. The obtained sample was dried and calcined at 600 ºC for 2 h heating at 2 ºC min^{-1} rate. Then it was reduced at 600 ºC heating at 2 ºC min^{-1} and kept for 2 h. The prepared catalyst was placed in a vacuum drying chamber for use.

Material characterizations: X-Ray diffraction (XRD) was performed at a DX-1000 diffractometer with Cu Kα radiation. The XRD patterns were recorded from 10 º to 80 º with 0.06 º step size. Raman was carried out at HOLIBAR-XploRA Plus instrument with an excitation wavelength of 532 nm. Thermogravimetric analysis was performed on NETZSCH STA 449 F5 analyzer equipped with mass spectrometer of QMS 403 D (TGA-MS). H_2 temperature-programmed reduction (H_2-TPR) was carried out using Micromeritics Autochem II 2920 instrument. The spectra were collected with 5 scans in the range of 100-3000 cm^{-1}. X-Ray photoelectron spectroscopy (XPS) was operated on AXIS Ultra DLD (KRATOS) spectrometer with monochromated Al radiation. The spectra were calibrated by C1s of 284.6 eV and fitted using XPSPEA41 software. Transmission electron microscopy (TEM) was carried out at FEI Talos F200 A electron microscope with an accelerating voltage of 200 kV. The sample was dispersed into ethanol and had an ultrasonic treatment, then dripped on copper grid coated with carbon films. Scan electron microscopy (SEM) was performed at JSM-7500F with an accelerating voltage of 20 kV. Fast ion bombardment using Ga^+ ions was performed to acquire images of cross-sections through the Ni_3Mo_3N crystals. H_2 chemisorption and NH_3 temperature-programed desorption (NH_3-TPD) were also performed at Micromeritics Autochem II 2920 instrument. Typically, approxmately 0.1 g sample was pretreated at 400 °C for 1 h in 10 % H_2/Ar and then 1 h in Ar. After cooled down to target

temperatures and treated in 10 % H_2/Ar or 10 % NH_3/He until becoming saturated, the sample was treated under Ar or He for 2 h and then heated to 600 °C for desorption. The total acid amount was calculated using a calibration file obtained by a quantitative loop. The calibration file was obtained by gas calibration and TCD calibration options on Micromeritics Autochem II 2920 instrument. According to the known NH_3 content of 10 % NH_3/He, the goodness of fit of the calibration file was restricted to values below ½ % maximum concentration. After performing the NH_3-TPD experiments, the total acidic density can be obtained on the instrument based on the peak area of desorption curve and catalyst amount.

Activity test: The conversion of palmitic acid was performed on a 300 mL Parr reactor (Parr instruments model 4484). Typically, 1.0 g palmitic acid, 0.1 g catalyst, 100 mL dodecane were added into the reactor. After sealing the reactor, 2.0 MPa N_2 was used to replace the air and then 2.0 MPa H_2 to replace N_2 in the reactor three times, respectively. The reactor was heated to target temperature rapidly and the reaction was timed. Circulating water system was used to balance the temperature of reactor. The course of the reaction was following by sampling periodically 0.5 mL of the reaction mixture that was analyzed immediately by gas chromatography (GC, PANNA A91). The instrument was equipped with a HP-5 column (30 m × 0.25 mm × 0.25 μm) and flame ionization detector (FID). The detection program was the following: 70 ºC, kept for 3 min, 70-160 ºC, 5 ºC min^{-1}, kept for 3 min, 160-230 ºC, 10 ºC min^{-1}, kept for 5 min, 230-280 ºC, 10 ºC min^{-1}, kept for 4 min. An internal standard method with tridecane as internal standard was used to quantify the composition of product. The gas products were detected by PANNA A91 gas chromatograph with a TCD detector and packed C-2000 column. The conversion, selectivity and yield of each component was calculated by the following equation:

Conversion (%) = $(1-C/C_0) \times 100\%$, where C and C_0 are the contents of palmitic acid in the product and reactant, respectively.

Selectivity (%) = $[n_i/(n_0-n)] \times 100\%$, where n_i, n_0 and n are the mole of product, the mole of palmitic acid in the reactant and product, accordingly.

Yield (%) = Conversion × Selectivity.

Initial reaction rates were calculated as follows:

$r_0 = (Conv. \times n_{Pal})/(g_{Catal} \times t)$, Conv. and n_{Pal} are conversion and initial amount of palmitic acid, respectively, g_{Catal} is the amount of catalyst and t corresponds to time. The initial reaction rate is calculated at t = 30 min.

From initial reaction rates, turnover frequency values (TOF) were estimated by dividing by the number of sites. Active sites are Ni and Mo atoms in the catalyst.

3. Results and discussion

3.1. Synthesis strategy of Ni_3Mo_3N catalyst

The traditional preparation method for metal nitrides is temperature programmed reaction between metal oxides and NH_3.[19] However, this method presents as major drawbacks the harsh reaction conditions due to the chemical stability of oxides, the slow reaction and the incomplete conversion of the oxide into nitride.[27, 28] Considering these limitations, preparation methodologies different from the conversion of structurally robust oxides into nitrides are much wanted.

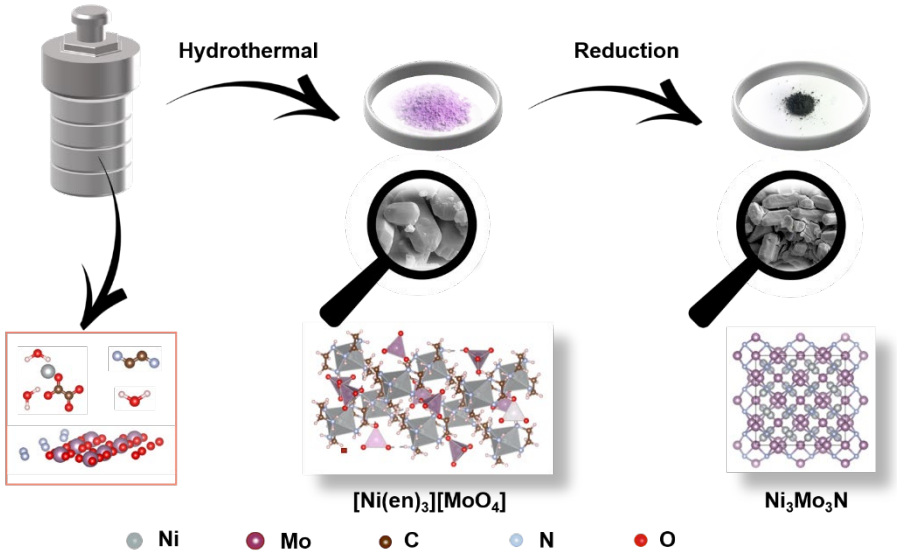

Scheme 1. Route for the preparation of Ni_3Mo_3N catalyst using hydrothermal and temperature-programed reduction methods.

In this context, the present study discloses a novel procedure for the synthesis of a bimetallic metal nitride, whose concept is based on the thermal transformation under reductive conditions of a salt consisting of a cationic nitrogenated complex of an oxyanion. The nitrogenated ligand of the metal cation should act as N source in the nitride formation. The two metals are forming part of the cation and the anion of the salt, respectively. Specifically, the synthesis of the Ni_3Mo_3N was performed in two steps as illustrated in **Scheme 1**. It consists in the formation of a molybdate intermediate containing Ni^{2+} and nitrogen, followed by its reductive thermal decomposition. The presence of H_2 during the synthesis should assist deoxygenation of oxyphilic molybdate by H_2O formation.

The key point of the synthesis is the pyrolysis of a nickel molybdate in which the Ni^{2+} ions form an octahedral complex with ethylenediamine (en). In this way, it was anticipated that the precursor containing Ni, Mo and N could evolve upon thermal treatment at high temperature in the presence of H_2 into the corresponding bimetallic nitride. The selection of

en, as a bidentate ligand to complex Ni^{2+} cations was based on the wide use of en in the controllable fabrication of nanomaterials.[29] There are precedents in the literature showing the synthesis of PbS with rod-shape using en as modulator.[30] The formed PbS rods are well crystallized with a relatively large aspect ratio and their performance derive in part from its morphology.

The $[Ni(en)_3][MoO_4]$ precursor with specific morphology could be prepared by a hydrothermal method consisting in the simultaneous formation of $Ni(en)_3^{2+}$ complex and ion metathesis of NH_4^+ by $Ni(en)_3^{2+}$ in $(NH_4)_6Mo_7O_{24}$. In the present case, we reasoned that the preparation of a bimetallic nitride in the temperature-programmed reduction process requires a precursor with a sufficiently high N content, like en. On the other hand, the small molecular size of en is conducive to the coordination of three ligands around the Ni^{2+} cation, increasing the total N content of the salt. In the present case, it was found that in the Ni molybdate salt, three en ligands coordinate to each Ni^{2+} cation, giving a high N percentage of the salt. Therefore, en appears as a suitable ligand for the preparation of $[Ni(en)_3][MoO_4]$ intermediate that could be transformed into a metal nitride.

3.2. Microstructures of Ni_3Mo_3N catalyst

Chemical analysis data and powder XRD confirm the successful formation of $[Ni(en)_3][MoO_4]$. **Figure 1** shows the XRD pattern recorded for $[Ni(en)_3][MoO_4]$ that agrees with the diffraction pattern corresponding to this salt (PDF#00-039-1904).

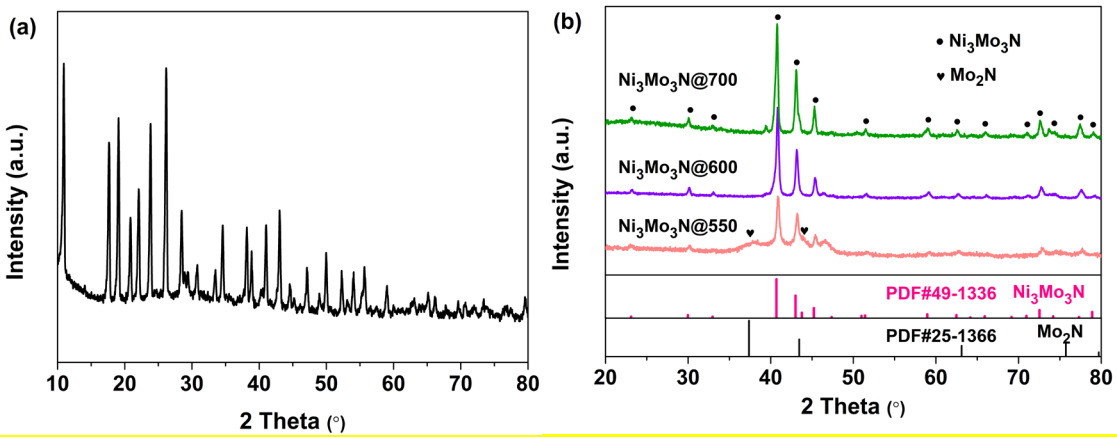

Figure 1. XRD data of (a) $[Ni(en)_3][MoO_4]$, (b) samples obtained at different temperatures.

Transformation of $[Ni(en)_3][MoO_4]$ into Ni_3Mo_3N was performed by thermal treatment under H_2 flow to favor molybdate reduction. Thermogravimetric analysis (TGA) coupled with differential scanning calorimetry provides a useful information about the thermal conversion of $[Ni(en)_3][MoO_4]$ into Ni_3Mo_3N. The results are presented in **Figure 2(a)**. TGA of $[Ni(en)_3][MoO_4]$ shows an abrupt weight loss starting at 300 ºC and ending approximately at 400 ºC of about 60-62 wt.%. Theoretically, the conversion of $[Ni(en)_3][MoO_4]$ into Ni_3Mo_3N would correspond to a weight loss of 60.04 %, very much close to the experimental value. This weight loss corresponds to two sharp peaks with maxima at 304 and 318 ºC, indicating the occurrence of a chemical reaction. Analysis by mass spectrometry of the gases evolved shows that CO was the major compound responsible for the weight loss, followed in much lesser extent by H_2O and NH_3. **Figure 2(b)** provides a summary of these analyses. Thermoprogrammed H_2 reduction of $[Ni(en)_3][MoO_4]$ also shows a strong sharp H_2 adsorption peak at 337 ºC, followed by a symmetric desorption peak at 387 ºC indicating that the $[Ni(en)_3][MoO_4]$ salt reacts with H_2 at the temperature range in which this salt decomposes desorbing H_2 and also releasing other gases, such as CO, CH_4 and C_2H_6. Gaseous H_2O and NH_3 evolved in the process are removed by a cold trap and are not detected (see **Figure S1** in supporting information). The combination of the information of

TGA, showing the decomposition of $[Ni(en)_3][MoO_4]$ together with the sharp H_2 uptake can serve to rationalize the successful synthesis of Ni_3Mo_3N from $[Ni(en)_3][MoO_4]$ under H_2 depicted in **Scheme 1**. Note that the gases measured in the TGA are probably different from those generated in the H_2 treatment.

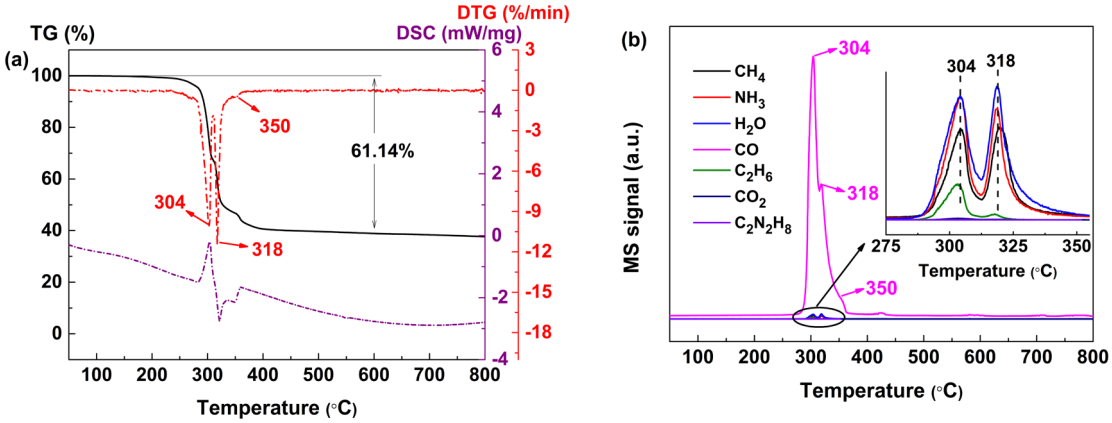

Figure 2. (a) TGA and DSC curves and (b) MS signals of $[Ni(en)_3][MoO_4]$ transformation in H_2 atmosphere.

Table 1. Crystal phases and crystallite size of the different catalysts from XRD.

Catalysts	Phase(s)		Crystallite size (nm)[a]	
Ni_3Mo_3N@550	Ni_3Mo_3N	Mo_2N	21.9	19.0
Ni_3Mo_3N@600	Ni_3Mo_3N		24.3	
Ni_3Mo_3N@700	Ni_3Mo_3N		26.3	

[a] Determined applying the Scherrer equation.

Samples of Ni_3Mo_3N prepared at 550, 600 and 700 ºC were characterized by powder XRD. The corresponding XRD patterns are also presented in **Figure 1**. Analysis of these diffractograms shows that $[Ni(en)_3][MoO_4]$ is converted into Ni_3Mo_3N for treatments at 600 and 700 ºC, the average crystallite size increasing with the temperature, while a mixture of Ni_3Mo_3N and Mo_2N is formed at 550 ºC. **Table 1** summarizes the results based on XRD analysis.

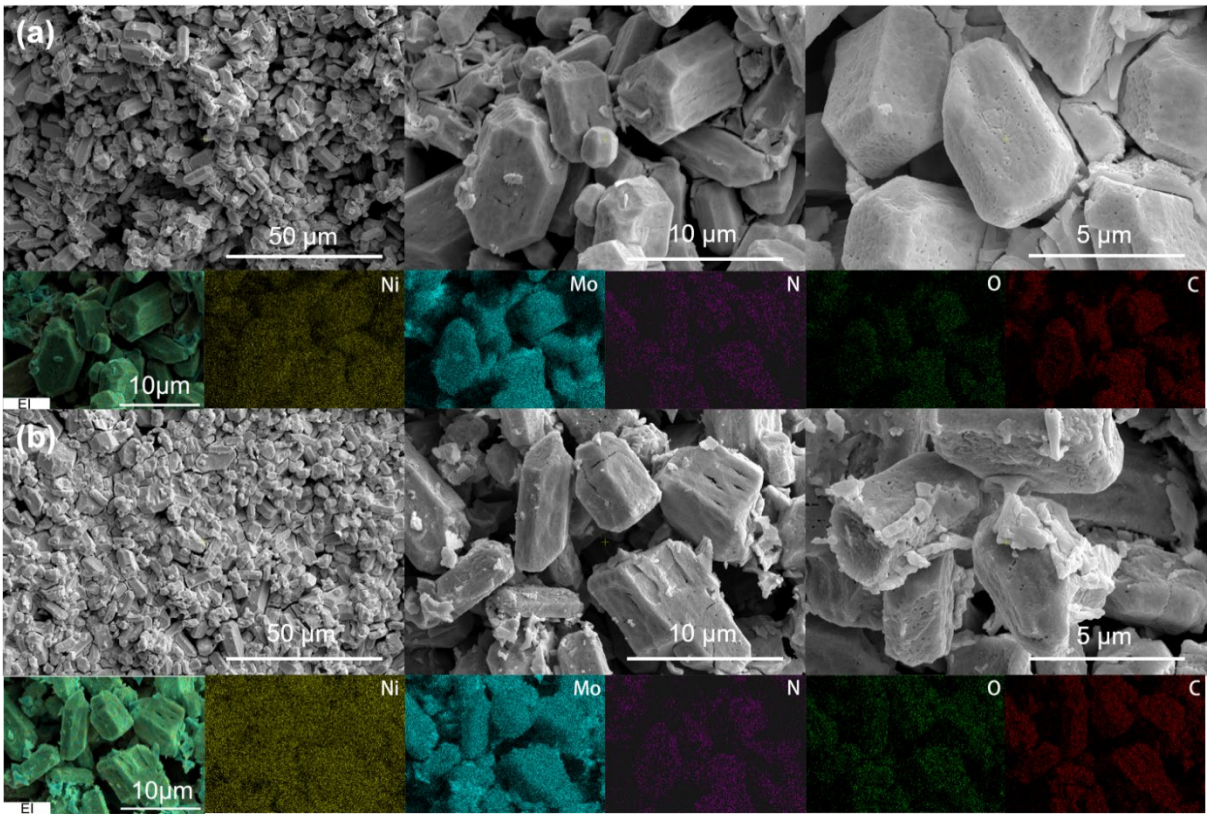

Figure 3. FESEM images and EDX element mappings including Ni, Mo, N, O and C of (a) Ni_3Mo_3N@600 and (b) Ni_3Mo_3N@700 catalysts.

The morphology of Ni_3Mo_3N samples obtained at 600 ºC was monitored by FESEM. The images provided in **Figure 3** show particles with well-defined geometry of truncated rhombohedra. Similar shapes are also observed for the Ni_3Mo_3N sample obtained at 550 (**Figure S2**) and 700 ºC, although in this case the FESEM images, also shown in **Figure 3**, reveal the presence of some debris, probably formed in the decomposition of large crystallites. Elemental mapping by EDS shows the coincidence of Ni and Mo at the micrometric scale, in agreement with the bimetallic nature of Ni_3Mo_3N. Fast ion bombardment using Ga^+ ions allows to acquire images of cross-sections through the Ni_3Mo_3N crystals. These images provided in **Figure 4** reveal that the particles are dense material, although eventually they can present some cavities or voids inside. HRTEM image shows a lattice space of 0.22 nm, which corresponds to the (211) plane of Ni_3Mo_3N.

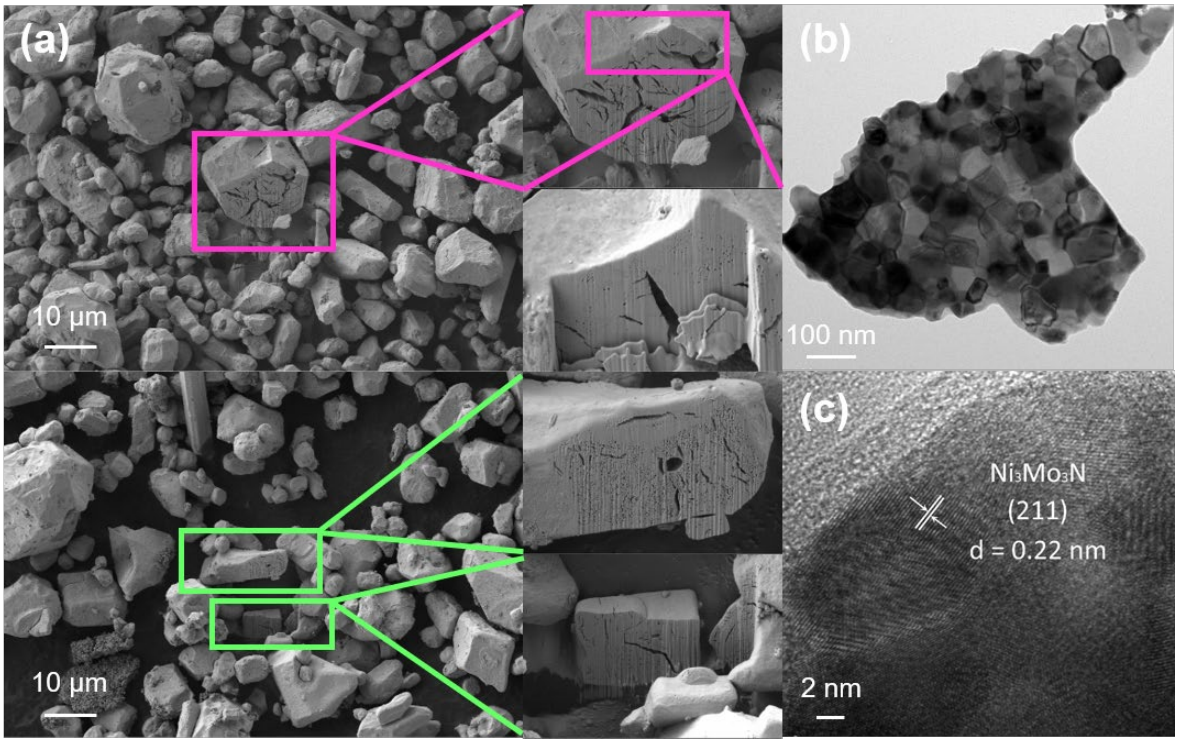

Figure 4. (a) FIB-SEM images, (b) TEM and (c) HRTEM images of Ni_3Mo_3N@600 catalyst.

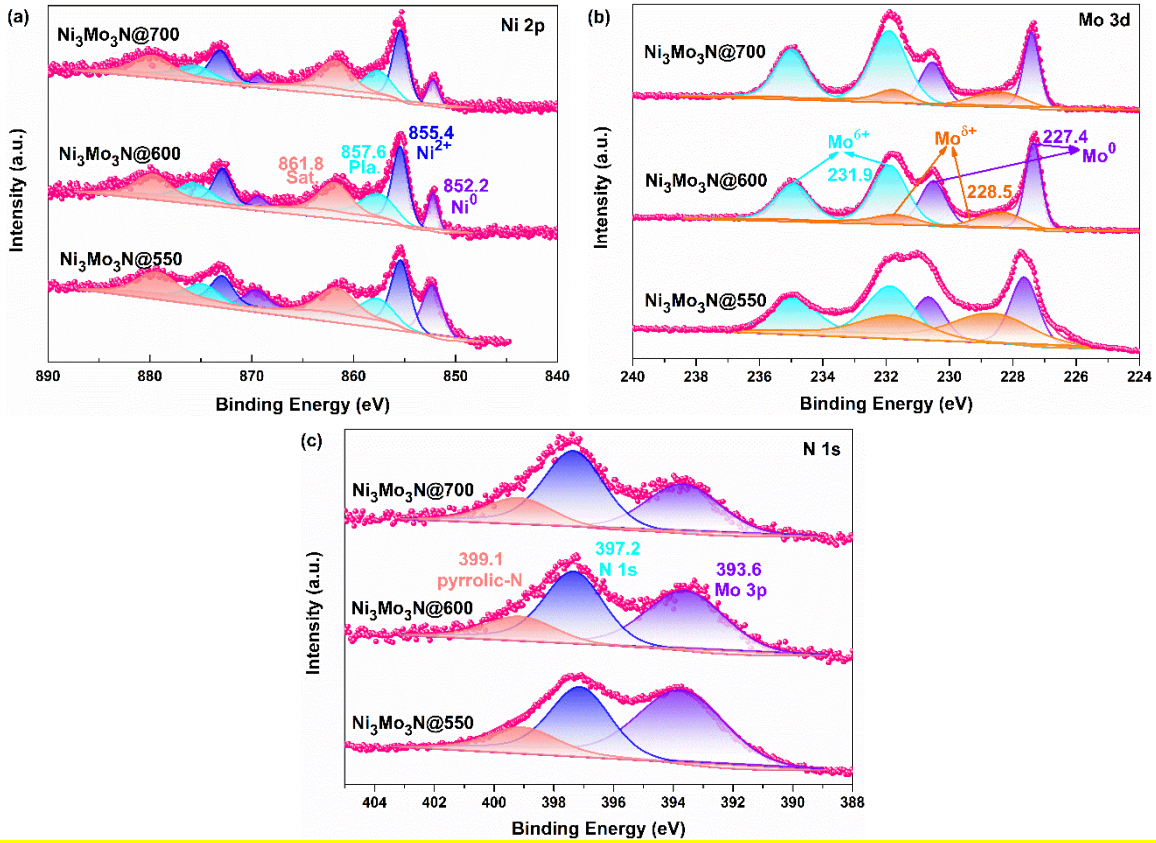

Figure 5. XPS spectra of (a) Ni 2p, (b) Mo 3d, and (c) N 1s regions of Ni_3Mo_3N@600 and Ni_3Mo_3N@700 catalysts.

Survey XPS spectra for Ni_3Mo_3N obtained at different temperatures show the peaks corresponding to the expected elements plus oxygen and carbon. **Figure 5** shows the experimental high resolution XPS peaks corresponding to Ni 2p, Mo 3d and N 1s levels for Ni_3Mo_3N samples prepared at 550, 600 and 700 ºC, while **Figure S3** in supporting information contains the survey spectra measured to the series of Ni_3Mo_3N samples, as well as the XPS peaks corresponding to O 1s and C 1s for both samples. **Table S1-S2** in supporting information summarizes the components, the binding energy values and proportions of the various components for each element, determined from the best deconvolution of the XPS peaks. As it can be seen there, the XPS Ni 2p peak recorded for the Ni_3Mo_3N obtained at 600 ºC can be deconvoluted into two components corresponding to Ni^0

and Ni^{2+} at 852.2 and 855.4 eV, respectively.[31, 32] Analogously, the experimental XPS Mo 3d peak for the same Ni_3Mo_3N sample at 600 ºC could be adequately fitted to three components appearing at binding energy values of 227.4, 228.5 and 231.9 eV attributable to Mo^0 and two positive Mo species.[33, 34] The binding energy values for Ni 2p and Mo 3d measured for the three Ni_3Mo_3N are about 0.4 and 0.6 eV lower than those of metallic Ni and Mo, respectively. This suggests that Ni and Mo atoms have somewhat higher electron density in Ni_3Mo_3N than in the pure metallic elements. The N 1s provides an important information, since it shows two components at binding energy values of 397.2 and 399.1 eV that correspond to the values expected for the metal nitride and pyrrolic N, respectively.[35, 36] Importantly, Ni_3Mo_3N sample prepared at 550 and 700 ºC shows the same components with coincident binding energy values and similar proportions as those determined for the Ni_3Mo_3N sample obtained at 600 ºC.

An interesting fact to comment is the observation of O 1s peak in the samples. This indicates that the external surface of the particles analyzed has become passivated. It should be noted at this point that the preparation procedure of NiMoN samples has a step of surface passivation by 5% O_2 in He to protect the surface. In fact, the main O component appears at 530.0 eV, which corresponds to O atoms in Ni-O and Mo-O metal oxide, while the other two components correspond to O bonded to C through a single (531.2 eV) or double (532.3 eV) bond.[37, 38] The C element at the surface can correspond to residual percentages of en or to ambient contamination and its deconvolution agrees with C-C, C-O and C=O coordination.[39] Since the XRD patterns previously commented show that the only phase for the samples prepared at 600 and 700 ºC corresponds Ni_3Mo_3N and considering the fact that XPS is a surface technique that does not provide information of the bulk particles, the combined information of XRD and XPS is compatible with the presence of metallic Ni and Mo atoms

characteristic of highly crystalline Ni_3Mo_3N particles that have undergo surface passivation by oxygen.

The presence of surface Mo-O together with Mo-N was also inferred from Raman spectra of the Ni_3Mo_3N samples, by recording the characteristic stretching and deformation vibrations.[40, 41] **Figure S4** in supporting information shows an expansion of the relevant low frequency region of the Raman spectra acquired for Ni_3Mo_3N at 550, 600 and 700 ºC. Interestingly, the wavenumber of the Mo-O vibration on the Ni_3Mo_3N surface is red shifted by about 15 cm^{-1} respect to the analogous peak appearing in the precursor.[41, 42] This could reflect the influence of Ni_3Mo_3N donating electron density to the Mo-O bonds.

3.3. Catalytic hydrodeoxygenation of palmitic acid

According to the known structure of Ni_3Mo_3N, the material contains Ni-Ni bonds as well as Ni-Mo and Mo-N bonds,[33, 43] Thus, the bimetallic nitride can be in a certain way considered as a Ni-Mo metal alloy in which the electronic density has been modulated by the presence of N atoms in lesser proportion. This is confirmed by the downshift of the binding energy values for Ni and Mo in Ni_3Mo_3N compared to pure metallic elements. The *quasi* metallic nature of Ni_3Mo_3N also explains that the external surface could become passivated in the preparation procedure upon exposure to 5 % O_2 in He for 10 h or upon prolonged storage under ambient oxygen. Not surprisingly in base to the structure of Ni_3Mo_3N and the existing bonds, Ni_3Mo_3N exhibits activity in hydrotreatment to remove S, N and O from oil fractions in petrochemistry and other reactions requiring H_2.[44]

Hydrogenation of palmitic acid dissolved in 100 mL dodecane was carried out in a 300 mL autoclave with mechanical stirring under 2 MPa H_2 pressure. A substrate/catalyst weight ratio of 10 was selected for most of the experiments. Preliminary controls under the same reaction conditions showed no conversion in the absence of catalyst or in its presence in

the absence of H_2. In contrast, using any of the Ni_3Mo_3N samples as catalyst, palmitic acid was converted to a mixture of hexadecanal, 1-hexadecanol, hexadecane and pentadecane. Under the reaction conditions, the removal of surface oxide detected by EDX and XPS is not expected to occur. Palmitic acid conversion depended on the catalyst, the Ni_3Mo_3N sample prepared at 700 ºC, being the less active, while those obtained at 550 and 600 ºC exhibiting similar initial reaction rate about 25 $mmol_{palmitic\ acid}\ g_{catalyst}^{-1}\ h^{-1}$. **Table S3** summarizes activity data for the samples under study. It is proposed that the larger particle size of Ni_3Mo_3N@700 and the difference surface composition respect to Ni_3Mo_3N@600 are responsible for the lower activity of the sample prepared at the highest decomposition temperature.

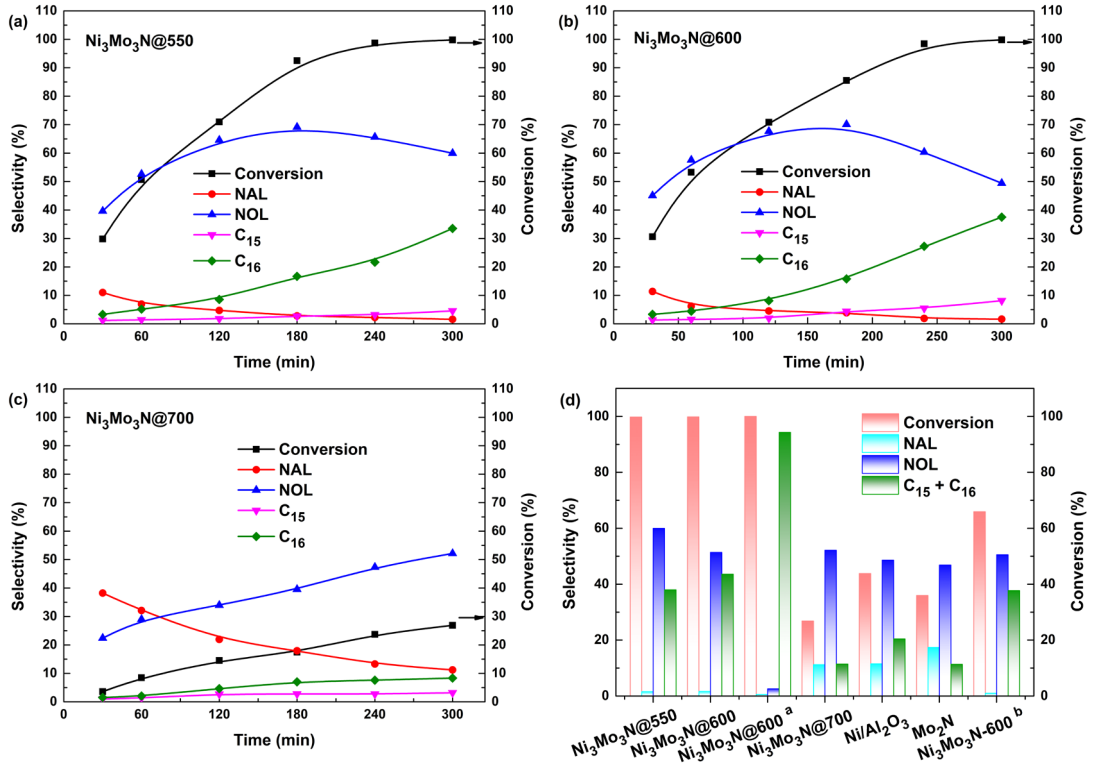

Figure 6. Palmitic acid conversion and selectivity of several products on the Ni_3Mo_3N catalysts prepared at different temperatures as well as benchmark catalysts such as Ni/Al_2O_3, Mo_2N and Ni_3Mo_3N-600 prepared by nitridation wiht NH_3. NOL represents 1-hexadecanol,

NAL represents hexadecanal. Reaction conditions: 0.1 g catalyst, 1.0 g palmitic acid, 270 ºC, 2.0 MPa H_2, 5 h. [a] 10 h reaction.

Product selectivity changed with conversion. **Figure 6** shows the temporal profile for the most active Ni_3Mo_3N catalyst in the series prepared at 600 ºC and the conversion and product selectivity at 5 h reaction time, while **Figure S5** in supporting information shows longer reaction times as well as the temporal product profiles for the other reactants. Time-yield plots for the products indicate that the aldehyde and the alcohol are primary, but unstable products. In comparison, hexa- and pentadecane appear as secondary and stable product. This is further confirmed by extending the reaction time beyond complete palmitic acid conversion up to 10 h and observing the complete transformation of 1-hexadecanol into hexadecane (**Figure S5**). Therefore, the hydrogenation kinetics follows the sequence indicated in **Scheme 2**. The combined selectivity for the C_{15}+C_{16} alkanes at 5 h reaction time was 44 and 38 % for Ni_3Mo_3N prepared at 600 and 550 ºC, respectively (**Table S3**). To put the catalytic activity of Ni_3Mo_3N into context, the activity of Ni supported on alumina (Ni/Al_2O_3, see experimental section for preparation and composition) as a benchmark catalyst was also tested under the reaction conditions. Other related materials also tested as catalysts are Mo_2N and an alternative Ni_3Mo_3N (Ni_3Mo_3N-600) sample obtained by nitridation with NH_3 of MoO_3 and $NiMoO_4$ at 700 and 600 ºC, respectively. The results for Ni/Al_2O_3, Mo_2N and Ni_3Mo_3N-600 are also included in **Figure 6**. As it can be seen there, Ni/Al_2O_3 and Mo_2N afford less than 40 % conversion with a combined selectivity to alkanes lower than 20 % that is much less than the 100 % palmitic conversion and over 40 % alkane selectivity achieved with Ni_3Mo_3N. Although Ni_3Mo_3N-600 performs somewhat better, palmitic acid conversion was still below 70 % with ess than 40 % alkane selectivity, compared with the 100 % conversion achieved for Ni_3Mo_3N-@600 (Figure 6). This comparison shows the advantage of

having a mixed Ni and Mo catalyst and the advantages of the $[Ni(en)_3][MoO_4]$ decomposition method over nitridation of the corresponding oxides. The better performance of Ni_3Mo_3N@600 over Ni_3Mo_3N-600 could derive from a more uniform N distribution throughout the solid in the material prepared by $[Ni(en)_3][MoO_4]$ decomposition and the use of H_2 in the synthesis that should reduce Ni and Mo to their metallic state. To have a broader context, **Table S4** in the supporting information compares the activity of the best Ni_3Mo_3N sample in the present study with other reported catalysts for palmitic acid hydrodeoxygenation. Excluding catalysts containing Pd, Ni_3Mo_3N compares favorably with the most active Ni catalysts reported so far, but working at much lower temperature (270 ºC) in comparison with 10% Ni/SiO_2 (380 ºC) [45] or giving much higher alkane selectivity than 20% Ni/ZrO_2 (66 %).[46]

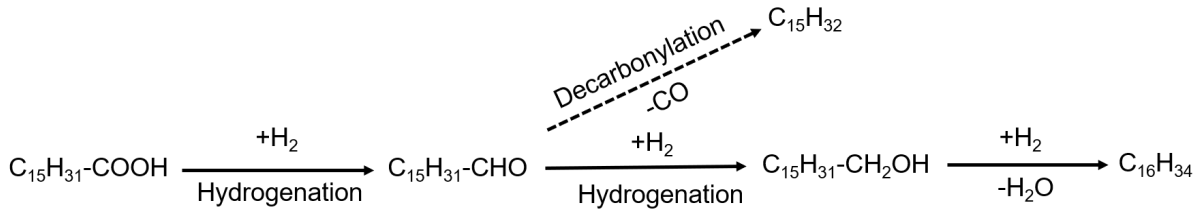

Scheme 2. The proposed reaction mechanism of palmitic acid on Ni_3Mo_3N@600 catalyst.

Activation energy for the Ni_3Mo_3N catalysts prepared at 600 and 700 ºC was determined from the Arrhenius plot of the natural logarithm of the initial reaction rate vs. the inverse of the absolute temperature in the range of reaction temperatures from 200 to 280 ºC. **Figure S6** shows the dependence of the reaction rate with the temperature. It was estimated that the activation energy of the sample prepared at 600 ºC was 45.4 kJ mol^{-1}, lower than that determined for the sample prepared at 700 ºC that was 65.7 kJ mol^{-1}, as shown in **Figure S7**. These values are lower than those previously reported in the literature for the activation energy of fatty acid hydrogenation using related Ni catalysts.[47, 48]

Reusability of the most active Ni_3Mo_3N catalyst was studied by performing five consecutive uses of the same sample. A summary of the results is presented in **Figure 7**. As it can be observed there, almost coincident temporal profiles of palmitic acid conversion were measured in the five runs. In addition, similar product distribution was determined at 10 h reaction with a minor decay in the combined percentage of alkanes from 95 to 89 % that is

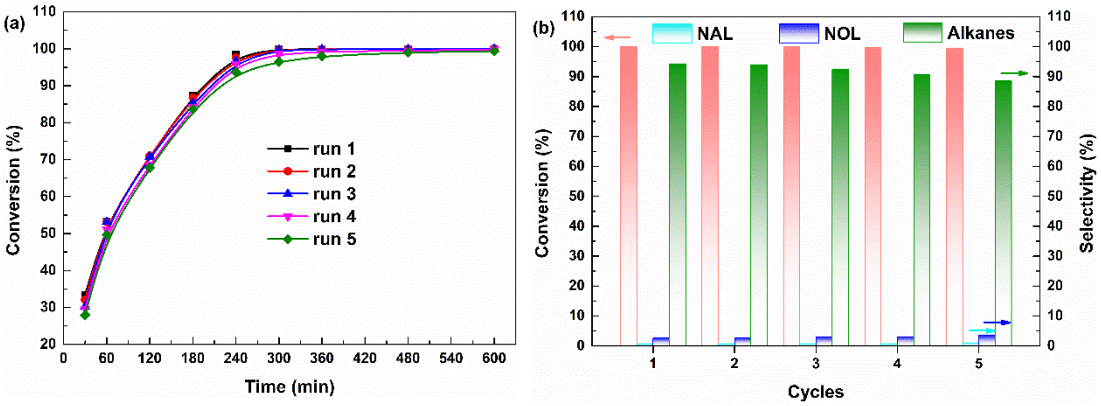

Figure 7. The stability of palmitic acid conversion and selectivity over Ni_3Mo_3N@600 catalyst. NOL represents 1-hexadecanol, NAL represents hexadecanal. Reaction conditions: 0.1 g catalyst, 1 g palmitic acid, 100 mL dodecane, 270 ºC, 2.0 MPa H_2, 10 h.

accompanied by a concomitant slight increase of 1-hexadecanol. Chemical analysis of the supernatant revealed that the combined Ni amount in the liquid phase of the five runs is below 5% of the total Ni content of Ni_3Mo_3N, while no changes in the chemical analysis, XRD patterns, Raman spectra and XPS analysis of the five times used sample were observed. **Figure S8-S10** present the spectroscopic data of five times used Ni_3Mo_3N sample. Altogether, the available experimental data indicates that Ni_3Mo_3N exhibits a remarkable catalytic stability with a minor decrease in catalytic activity, particularly in the conversion of hydrodeoxygenation of 1-hexadecanol to hexadecane. This slight catalyst deactivation could be due to the neutralization of some acid sites during the course of the reaction. This partial neutralization is frequently observed for other solid acids in which the acid sites are poisoned

by byproducts, cationic species or even coke. (Corma, A.; García, H.,A unified approach to zeolites as acid catalysts and as supramolecular hosts exemplified, *Journal of the Chemical Society, Dalton Transactions* **2000**, 1381-1394) Hydrodeoxygation of alcohols and ethers is a process widely reported in biomass transformation and is known to require of bifunctional catalysts containing metal sites to activate molecular H_2 and acid sites to facilitate the cleavage of C-O bonds. [49] In the present case, the acidity of palmitic acid could also assist the process. To further confirm this proposal on the mechanism of catalyst deactivation, hydrogenation of palmitic acid was also carried out in the presence of pyridine, as shown in **Figure S11**. The conversion of palmitic acid was 96 % at 5 h, which was similar with that in the absence of pyridine. However, the selectivity of hexadecanol almost remained constant at about 67%, while C_{15} and C_{16} increased slightly. This result indicated that the reaction was blocked in the transformation of hexadecanol to alkanes and supported that catalyst deactivation derives mainly from the neutralization of acid sites. These acid sites are mostly required for hexadecanol transformation, but not for palmitic acid hydrogenation to hexadecanal and, then, to 1-hexadecanol.

3.4. Reaction mechanism of Ni_3Mo_3N

As shown in **Scheme 2**, product evolution indicates that hydrodeoxygenation proceeds through a series of steps that are initiated by the reduction of carboxylic acid to the corresponding aldehyde, followed by a second hydrogenation to alcohol. The last step is hydrogenative dehydroxylation of 1-hexadecanol to hexadecane, as confirmed at longer reaction times (**Figure S5**). Alternative, hexadecanal can undergo decarbonylation to pentadecane. Some evidence supporting decarbonylation vs. decarboxylation has been the observation in the head space of CH4 evolution (by catalytic CO hydrogenation) as determined by gas chromatography (**Figure S13**). 1-Hexadecanol can also afford C_{15} by

hydrogenative C-C bond cleavage of the terminal alcohol. This mechanistic proposal agrees with the common observation that alcohols are the final product of fatty acid hydrogenation, through the intermediacy of the corresponding aldehyde.[50] This proposal was supported by performing analogous hydrodeoxygenations in the presence of Ni_3Mo_3N as catalyst replacing palmitic acid by hexadecanal or 1-hexadecanol as starting materials. The results are presented in **Figure S5**. As it can be seen there, starting from hexadecanal, 1-hexadecanol is a primary and unstable product formed with high initial selectivity. In the case of 1-hexadecanol, C_{15} appears as a very minor product. Importantly, comparison of the reaction temporal profiles indicates that 1-hexadecanol reaction is the slowest in the pathway indicated in **Scheme 2**.

As commented earlier, precedents in the literature have suggested that hydrodeoxygenation requires bifunctional catalysts that combine acid centers and hydrogenation sites.[49] To provide evidence of the presence of both types of sites in the Ni_3Mo_3N that could serve to rationalize their relative catalytic activity, a series of thermoprogramed NH_3 desorption measurements to determine the density and strength of acid sites and H_2 chemisorption studies to analyze the interaction of H_2 with the materials were performed. The corresponding desorption or adsorption plots as a function of the temperature are provided in **Figure S12**, while **Table 2** summarizes the results. As it can be seen there, the density of acid centers and the specific H_2 chemisorption decreases along with the synthesis temperature. This trend can be interpreted considering that as the crystallinity of the Ni_3Mo_3N increases with the synthesis temperature and the structural defects diminish, the density of acid sites and H_2 chemisorption decreases. Acid sites are proposed to derive from structural defects including oxygenated M-OH groups, coordinatively unsaturated metal sites and atom vacancies. Therefore, acidity and H_2 chemisorption appear associated to structural defects. The high catalytic activity of Ni_3Mo_3N prepared at 550 ºC can be associated to structural

defects, acidity and H_2 chemisorption, while the low activity of Ni_3Mo_3N prepared at 700 ºC is due to the low density of acid sites and poor H_2 chemisorption.

Table 2. Acid sites and H-sites data of different catalysts, acid sites are determined by NH_3-TPD, H-sites are determined by H_2 chemisorption.

Catalysts	Acid sites (μmol g^{-1})	H-sites (μmol g^{-1})	Acid : H site ratio
Ni_3Mo_3N@550	48.2	28.2	1.7
Ni_3Mo_3N@600	21.3	8.50	2.5
Ni_3Mo_3N@700	17.1	5.08	3.4

However, the catalytic activity of the Ni_3Mo_3N sample obtained at 600 ºC that is slightly better than that prepared at 550 ºC indicates that besides acidity and H_2 chemisorbed, other factors should also influence the performance of Ni_3Mo_3N. It is proposed that organic byproducts, polymeric substances or residual C content (Corma, A.; García, H.,A unified approach to zeolites as acid catalysts and as supramolecular hosts exemplified, *Journal of the Chemical Society, Dalton Transactions* **2000**, 1381-1394) and the presence of Mo_2N phase resulting from the incomplete conversion of $[Ni(en)_3][MoO_4]$ into Ni_3Mo_3N is also detrimental for the catalytic activity. Thus, the Ni_3Mo_3N sample prepared at 600 ºC represents a good balance of bifunctional site density and better developed structure with similar crystal size.

4. Conclusion

It is reported here that Ni_3Mo_3N is among the most efficient solid catalysts for hydrodeoxygenation of palmitic acid to C_{15}/C_{16} alkanes. The process is of interest in the preparation of synthetic gasoil with nearly no CO_2 footprint. The Ni_3Mo_3N samples used here have been prepared through a novel route that is based on the reductive decomposition of the molybdate salt of a Ni^{2+}-ethylenediamine coordination complex. In the decomposition, ethylenediamine acts as N source, while H_2 assists the reduction of oxophilic Mo. The dependence of the hydrodeoxygenation catalytic activity on the decomposition temperature of $[Ni(en)_3][MoO_4]$ has been rationalized as derived from the bifunctional acid and hydrogenating sites and the crystallinity of the material. The present results show how the structural robustness of molybdenum nitrides together with the possibility to prepare bimetallic materials are useful for the development of efficient solid catalysts for reactions requiring harsh conditions.

Corresponding Author

Changwei Hu - Key Laboratory of Green Chemistry and Technology, College of Chemistry, Sichuan University, 29 Wangjiang Road, Chengdu, 610064, P. R. China; Email: changweihu@scu.edu.cn

Hermenegildo Garcia - Instituto Universitario de Tecnología Química, Consejo Superior de Investigaciones Científicas.-Universitat Politecnica de Valencia, Universitat Politecnica de Valencia, Av. De los Naranjos s/n, 46022 Valencia, Spain; Email: hgarcia@qim.upv.es

Authors

Xiangze Du - Key Laboratory of Green Chemistry and Technology, College of Chemistry, Sichuan University, 29 Wangjiang Road, Chengdu, 610064, P. R. China; Instituto Universitario de Tecnología Química, Consejo Superior de Investigaciones Científicas.-

Universitat Politecnica de Valencia, Universitat Politecnica de Valencia, Av. De los Naranjos s/n, 46022 Valencia, Spain.

Xiaomei Lei - Key Laboratory of Green Chemistry and Technology, College of Chemistry, Sichuan University, 29 Wangjiang Road, Chengdu, 610064, P. R. China.

Linyuan Zhou - Key Laboratory of Green Chemistry and Technology, College of Chemistry, Sichuan University, 29 Wangjiang Road, Chengdu, 610064, P. R. China.

Yong Peng - Instituto Universitario de Tecnología Química, Consejo Superior de Investigaciones Científicas.-Universitat Politecnica de Valencia, Universitat Politecnica de Valencia, Av. De los Naranjos s/n, 46022 Valencia, Spain.

Yan Zeng - Key Laboratory of Green Chemistry and Technology, College of Chemistry, Sichuan University, 29 Wangjiang Road, Chengdu, 610064, P. R. China.

Huiru Yang - Key Laboratory of Green Chemistry and Technology, College of Chemistry, Sichuan University, 29 Wangjiang Road, Chengdu, 610064, P. R. China.

Dan Li - Key Laboratory of Green Chemistry and Technology, College of Chemistry, Sichuan University, 29 Wangjiang Road, Chengdu, 610064, P. R. China.

Author Contributions

The manuscript was written through contributions of all authors. All authors have given approval to the final version of the manuscript.

Notes

The authors declare no competing financial interest.

Supporting information

H_2-TPR curve (Figure S1), SEM images of Ni_3Mo_3N@550 sample (Figure S2), XPS spectra of survey, O 1s and C 1s regions (Figure S3), Raman spectra (Figure S4), temperal profiles of hexadecanal and hexadecanol conversion (Figure S5), kinetic data (Figure S6 and S7), XRD, Raman and XPS of used Ni_3Mo_3N@600 sample (Figure S8-10), temperal profile of palmitic acid conversion in the presence of pyridine (Figure S11), NH_3-TPD and H_2 chemisorption (Figure S12), XPS analysis data (Table S1and S2), activity performance (Table S3), summary of activity data of reported catalysts (Table S4), as well as references.

Acknowledgements

This work is financially supported by National Natural Science Foundation of China (No.21972099), the Application Foundation Program of Sichuan Province (No. 2021YJ0305), and 111 project (No. B17030). Financial support by the Spanish Ministry of Science and Innovation (Severo Ochoa and RTI2018-89237-CO2-R1) and Generalitat Valenciana are gratefully acknowledged. X. Du is also grateful for financial support from CSC (China Scholarship Council).

References

1. Santillan-Jimenez, E.; Crocker, M. Catalytic deoxygenation of fatty acids and their derivatives to hydrocarbon fuels via decarboxylation/decarbonylation. *J. Chem. Technol. Biotechnol.* **2012,** *87* (8), 1041-1050.

2. Pearlson, M.; Wollersheim, C.; Hileman, J. A techno-economic review of hydroprocessed renewable esters and fatty acids for jet fuel production. *Biofuel Bioprod Biorefin* **2013,** *7* (1), 89-96.

3. Canakci, M.; Van Gerpen, J. In A pilot plant to produce biodiesel from high free fatty acid feedstocks, 2001 ASAE Annual Meeting, American Society of Agricultural and Biological Engineers: 1998; p 1.

4. Ullrich, J.; Breit, B. Selective hydrogenation of carboxylic acids to alcohols or alkanes employing a heterogeneous catalyst. *ACS Catal.* **2018,** *8* (2), 785-789.

5. Cui, X.; Li, Y.; Topf, C.; Junge, K.; Beller, M. Direct Ruthenium-Catalyzed Hydrogenation of Carboxylic Acids to Alcohols. *Angew.Chem.Int.Ed.* **2015,** *54* (36), 10596-10599.

6. Tamura, M.; Nakagawa, Y.; Tomishige, K. Recent developments of heterogeneous catalysts for hydrogenation of carboxylic acids to their corresponding alcohols. *Asian J. Org. Chem.* **2020,** *9* (2), 126-143.

7. Manyar, H. G.; Paun, C.; Pilus, R.; Rooney, D. W.; Thompson, J. M.; Hardacre, C. Highly selective and efficient hydrogenation of carboxylic acids to alcohols using titania supported Pt catalysts. *Chem. commun.* **2010,** *46* (34), 6279-6281.

8. Climent, M. J.; Corma, A.; Iborra, S. Conversion of biomass platform molecules into fuel additives and liquid hydrocarbon fuels. *Green Chem.* **2014,** *16* (2), 516-547.

9. Klimmek, H. Influence of various catalyst poisons and other impurities on fatty acid hydrogenation. *J Am Oil Chem Soc* **1984,** *61* (2), 200-204.

10. Li, G.; Chen, L.; Fan, R.; Liu, D.; Chen, S.; Li, X.; Chung, K. H. Catalytic deoxygenation of C18 fatty acid over supported metal Ni catalysts promoted by the basic sites of $ZnAl_2O_4$ spinel phase. *Catal. Sci. Technol.* **2019,** *9* (1), 213-222.

11. Khalit, W. N. A. W.; Asikin-Mijan, N.; Marliza, T. S.; Gamal, M. S.; Shamsuddin, M. R.; Saiman, M. I.; Taufiq-Yap, Y. Catalytic deoxygenation of waste cooking oil utilizing nickel oxide catalysts over various supports to produce renewable diesel fuel. *Biomass Bioenergy* **2021,** *154*, 106248.

12. Giraldo, L.; Camargo, G.; Tirano, J.; Moreno-Pirajan, J. Synthesis of fatty alcohols from oil palm using a catalyst of Ni-Cu supported onto zeolite. *E-J. Chem.* **2010,** *7* (4), 1138-1147.

13. Ni, J.; Leng, W.; Mao, J.; Wang, J.; Lin, J.; Jiang, D.; Li, X. Tuning electron density of metal nickel by support defects in Ni/ZrO_2 for selective hydrogenation of fatty acids to alkanes and alcohols. *Appl. Catal. B* **2019,** *253*, 170-178.

14. Cheah, K. W.; Taylor, M. J.; Osatiashtiani, A.; Beaumont, S. K.; Nowakowski, D. J.; Yusup, S.; Bridgwater, A. V.; Kyriakou, G. Monometallic and bimetallic catalysts based on Pd, Cu and Ni for hydrogen transfer deoxygenation of a prototypical fatty acid to diesel range hydrocarbons. *Catal. Today* **2020,** *355*, 882-892.

15. Zhang, J.; Zhao, C. Development of a Bimetallic Pd-Ni/HZSM-5 Catalyst for the Tandem Limonene Dehydrogenation and Fatty Acid Deoxygenation to Alkanes and Arenes for Use as Biojet Fuel. *ACS Catal.* **2016,** *6* (7), 4512-4525.

16. Sajkowski, D. J.; Oyama, S. T. Catalytic hydrotreating by molybdenum carbide and nitride unsupported Mo_2N and Mo_2C/Al_2O_3. *Appl. Catal. A* **1996,** *134*, 339-349.

17. K.S. Weil; Kumta, P. N. Synthesis of ternary transition metal nitrides using chemically complexed precursors. *Mater. Sci. Eng. B* **1996,** *38*, 109-117.

18. Schaidle, J. A.; Thompson, L. T. Fischer-Tropsch synthesis over early transition metal carbides and nitrides: CO activation and chain growth. *J. Catal.* **2015,** *329*, 325-334.

19. R. Kojima; Aika, K. Molybdenum nitride and carbide catalysts for ammonia synthesis. *Appl. Catal. A* **2001,** *219*, 141-147.

20. Xie, J.; Li, S.; Zhang, X.; Zhang, J.; Wang, R.; Zhang, H.; Pan, B.; Xie, Y. Atomically-thin molybdenum nitride nanosheets with exposed active surface sites for efficient hydrogen evolution. *Chem. Sci.* **2014,** *5* (12), 4615-4620.

21. Ranhotra, G. S.; Bell, A. T.; Reimer, J. A. Catalysis over molybdenum carbides and nitrides: II. Studies of CO hydrogenation and C_2H_6 hydrogenolysis. *J. Catal.* **1987,** *108* (1), 40-49.

22. Sankar, M.; Dimitratos, N.; Miedziak, P. J.; Wells, P. P.; Kiely, C. J.; Hutchings, G. J. Designing bimetallic catalysts for a green and sustainable future. *Chem. Soc. Rev.* **2012,** *41* (24), 8099-8139.

23. Alonso, D. M.; Wettstein, S. G.; Dumesic, J. A. Bimetallic catalysts for upgrading of biomass to fuels and chemicals. *Chem. Soc. Rev.* **2012,** *41* (24), 8075-8098.

24. Chen, W. F.; Sasaki, K.; Ma, C.; Frenkel, A. I.; Marinkovic, N.; Muckerman, J. T.; Zhu, Y.; Adzic, R. R. Hydrogen-evolution catalysts based on non-noble metal nickel-molybdenum nitride nanosheets. *Angew Chem Int Ed Engl* **2012,** *51* (25), 6131-6135.

25. Chu, Y.; Wei, Z.; Yang, S.; Li, C.; Xin, Q.; Min, E. $NiMoN_x/\gamma$-Al_2O_3 catalyst for HDN of pyridine. *Appl. Catal. A* **1999,** *176*, 17-26.

26. Egorova, M.; Prins, R. The role of Ni and Co promoters in the simultaneous HDS of dibenzothiophene and HDN of amines over Mo/γ-Al_2O_3 catalysts. *J. Catal.* **2006,** *241* (1), 162-172.

27. Lei, M.; Zhao, H.; Yang, H.; Song, B.; Cao, L.; Li, P.; Tang, W. Syntheses of metal nitrides, metal carbides and rare-earth metal dioxymonocarbodiimides from metal oxides and dicyandiamide. *J. Alloys Compd.* **2008,** *460* (1-2), 130-137.

28. Buha, J.; Djerdj, I.; Antonietti, M.; Niederberger, M. Thermal transformation of metal oxide nanoparticles into nanocrystalline metal nitrides using cyanamide and urea as nitrogen source. *Chem. Mater.* **2007,** *19* (14), 3499-3505.

29. Soyama S. (nee Yokoi); M. I., Funahashi, S.; Tanaka, M. Variable-temperature and -pressure multinuclear magnetic resonance study of solvent exchange at the tris(ethylenediamine)nickel(II) ion in ethylenediamine. *Inorg. Chem.* **1992,** *31*, 536-538.

30. Chen, M.; Xie, Y. Yao, Z.; Qian, Y.; Zhou, G. A novel solvent-directed shape control technique for preparation of rod-shaped PbS crystals. *Mater. Res. Bull.* **2002,** *37*, 247-253.

31. Wang, Y.; Ling, Li.; Jiang, H. Selective hydrogenation of lignin to produce chemical commodities by using a biochar supported Ni-Mo_2C catalyst obtained from biomass. *Green Chem.* **2016,** *18* (14), 4032-4041.

32. Du, X.; Zhou, K.; Zhou, L.; Lei, X.; Yang, H.; Li, D.; Hu, C. Efficient catalytic conversion of jatropha oil to high grade biofuel on Ni-Mo_2C/MCM-41 catalysts with tuned surface properties. *J. Energy Chem.* **2021,** *61*, 425-435.

33. Chen, Y.; Yu, J.; Jia, J.; Liu, F.; Zhang, Y.; Xiong, G.; Zhang, R.; Yang, R.; Sun, D.; Liu, H.; Zhou, W. Metallic Ni_3Mo_3N Porous Microrods with Abundant Catalytic Sites as Efficient Electrocatalyst for Large Current Density and Superstability of Hydrogen Evolution Reaction and Water Splitting. *Appl. Catal. B* **2020,** *272*, 118956.

34. Böröczki, Á.; Dobos, G.; Josepovits, V. K.; Hárs, G. High temperature reactions between molybdenum and metal halides. *Appl. Surf. Sci.* **2006,** *252* (23), 8309-8313.

35. Li, M.; Zhu, Y.; Wang, H.; Wang, C.; Pinna, N.; Lu, X. Ni Strongly Coupled with Mo_2C Encapsulated in Nitrogen-Doped Carbon Nanofibers as Robust Bifunctional Catalyst for Overall Water Splitting. *Adv. Energy Mater.* **2019,** *9* (10), 1803185.

36. Yan, H.; Xie, Y.; Jiao, Y.; Wu, A.; Tian, C.; Zhang, X.; Wang, L.; Fu, H. Holey Reduced Graphene Oxide Coupled with an Mo_2N-Mo_2C Heterojunction for Efficient Hydrogen Evolution. *Adv. Mater.* **2018,** *30* (2), 1704156.

37. Du, X.; Li, N.; Zhang, X. Controlled synthesis of Co_3O_4@$NiMoO_4$ core-shell nanorod arrays for efficient water splitting. *Dalton Trans* **2018,** *47* (35), 12071-12074.

38. Wang, S.-G.; Lin, J.; Fan, C.-Y.; Li, Y.-F.; Zhang, J.-P.; Wu, X.-L.; Sun, H.-Z.; Deng, M.-X.; Su, Z.-M. Target encapsulating $NiMoO_4$ nanocrystals into 1D carbon nanofibers as free-standing anode material for lithium-ion batteries with enhanced cycle performance. *J. Alloys Compd.* **2020,** *830*, 154648.

39. Zhou, L.; Zeng, S.; Zheng, D.; Zeng, Y.; Wang, F.; Xu, W.; Liu, J.; Lu, X. $NiMoO_4$ nanowires supported on Ni/C nanosheets as high-performance cathode for stable aqueous rechargeable nickel-zinc battery. *Chem. Eng. J.* **2020,** *400*, 125832.

40. Ohta, N.; Scheuermann, W.; Nakamoto, K.; Matsuda, Y.; Yamada, S.; Murakami, Y. Resonance Raman Spectra of Tetrapyrrole Complexes of Oxomolybdenum(V). *Inorg. Chem.* **1979,** *18*, 457-460.

41. Xue, S.; Zhang, W.; Zhang, Q.; Du, J.; Cheng, H.-M.; Ren, W. Heterostructured Ni–Mo-N nanoparticles decorated on reduced graphene oxide as efficient and robust electrocatalyst for hydrogen evolution reaction. *Carbon* **2020,** *165*, 122-128.

42. Chen, Y. Y.; Zhang, Y.; Zhang, X.; Tang, T.; Luo, H.; Niu, S.; Dai, Z. H.; Wan, L. J.; Hu, J. S. Self-Templated Fabrication of $MoNi_4/MoO_{3-x}$ Nanorod Arrays with Dual Active Components for Highly Efficient Hydrogen Evolution. *Adv. Mater.* **2017,** *29* (39), 1703311.

43. Persson, K. Materials Data on Ni_3Mo_3N (SG:227) by Materials Project. **2016**.

44. Jaf, Z. N.; Miran, H. A.; Jiang, Z.-T.; Altarawneh, M. Molybdenum nitrides from structures to industrial applications. *Rev. Chem. Eng.* **2021,** 000010151520210002.

45. Xing, S.; Liu, Y.; Liu, X.; Li, M.; Fu, J.; Liu, P.; Lv, P.; Wang, Z. Solvent-free hydrodeoxygenation of bio-lipids into renewable alkanes over NiW bimetallic catalyst under mild conditions. *Appl. Catal. B.* **2020,** *269*, 118718.

46. Miao, C.; Marin-Flores, O.; Davidson, S. D.; Li, T.; Dong, T.; Gao, D.; Wang, Y.; Garcia-Pérez, M.; Chen, S. Hydrothermal catalytic deoxygenation of palmitic acid over nickel catalyst. *Fuel* **2016,** *166*, 302-308.

47. Peng, B.; Zhao, C.; Kasakov, S.; Foraita, S.; Lercher, J. A. Manipulating catalytic pathways: deoxygenation of palmitic acid on multifunctional catalysts. *Chemistry* **2013,** *19* (15), 4732-4741.

48. Yue, S.; Dong, L.; Liu, X.; Guo, Y.; Wang, Y. Hydrogenation of palmitic acid over Ni/Nb_2O_5-SiO_2 catalyst: Synergetic effect and kinetic study. *Ind Crops Prod* **2020,** *158*, 113006.

49. Voeste, T.; Buchold, H. Production of fatty alcohols from fatty acids. *J Am Oil Chem Soc* **1984,** *61* (2), 350-352.

50. Sun, D.; Sato, S.; Ueda, W.; Primo, A.; Garcia, H.; Corma, A. Production of C_4 and C_5 alcohols from biomass-derived materials. *Green Chem.* **2016,** *18* (9), 2579-2597.

Bimetallic Ni-Mo nitride is synthesized by a novel strategy using reductive decomposition of tris(ethylenediamine)nickel molybdate. Ni_3Mo_3N shows bifunctional properties in the hydrodeoxygenation of palmitic acid to alkanes efficiently. This study shows how the structural robustness of molybdenum nitrides together with the possibility to prepare bimetallic materials are useful for the development of efficient solid catalysts for reactions requiring harsh conditions.

X. Du, X. Lei, L. Zhou, Y. Peng, Y. Zeng, H. Yang, D. Li, C. Hu,* H Garcia*

Bimetallic Ni and Mo nitride as efficient catalyst for hydrodeoxygenation of palmitic acid

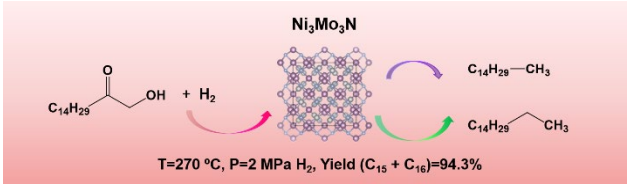

For Table of Contents Only

1. Santillan - Jimenez, E.; Crocker, M., Catalytic Deoxygenation of Fatty Acids and Their Derivatives to Hydrocarbon Fuels Via Decarboxylation/Decarbonylation. *J. Chem. Technol. Biotechnol.* **2012,** *87*, 1041-1050.
2. Pearlson, M.; Wollersheim, C.; Hileman, J., A Techno - Economic Review of Hydroprocessed Renewable Esters and Fatty Acids for Jet Fuel Production. *Biofuel Bioprod Biorefin* **2013,** *7*, 89-96.
3. Canakci, M.; Van Gerpen, J. In *A Pilot Plant to Produce Biodiesel from High Free Fatty Acid Feedstocks*, 2001 ASAE Annual Meeting, American Society of Agricultural and Biological Engineers: 1998; p 1.
4. Ullrich, J.; Breit, B., Selective Hydrogenation of Carboxylic Acids to Alcohols or Alkanes Employing a Heterogeneous Catalyst. *ACS Catal.* **2018,** *8*, 785-789.
5. Cui, X.; Li, Y.; Topf, C.; Junge, K.; Beller, M., Direct Ruthenium - Catalyzed Hydrogenation of Carboxylic Acids to Alcohols. *Angew.Chem.Int.Ed.* **2015,** *54*, 10596–10599.
6. Tamura, M.; Nakagawa, Y.; Tomishige, K., Recent Developments of Heterogeneous Catalysts for Hydrogenation of Carboxylic Acids to Their Corresponding Alcohols. *Asian J. Org. Chem.* **2020,** *9*, 126-143.
7. Manyar, H. G.; Paun, C.; Pilus, R.; Rooney, D. W.; Thompson, J. M.; Hardacre, C., Highly Selective and Efficient Hydrogenation of Carboxylic Acids to Alcohols Using Titania Supported Pt Catalysts. *Chem. commun.* **2010,** *46*, 6279-6281.
8. Climent, M. J.; Corma, A.; Iborra, S., Conversion of Biomass Platform Molecules into Fuel Additives and Liquid Hydrocarbon Fuels. *Green Chem.* **2014,** *16*, 516-547.

9. Klimmek, H., Influence of Various Catalyst Poisons and Other Impurities on Fatty Acid Hydrogenation. *J Am Oil Chem Soc* **1984,** *61*, 200-204.
10. Li, G.; Chen, L.; Fan, R.; Liu, D.; Chen, S.; Li, X.; Chung, K. H., Catalytic Deoxygenation of C18 Fatty Acid over Supported Metal Ni Catalysts Promoted by the Basic Sites of $Znal_2o_4$ Spinel Phase. *Catal. Sci. Technol.* **2019,** *9*, 213-222.
11. Khalit, W. N. A. W.; Asikin-Mijan, N.; Marliza, T. S.; Gamal, M. S.; Shamsuddin, M. R.; Saiman, M. I.; Taufiq-Yap, Y., Catalytic Deoxygenation of Waste Cooking Oil Utilizing Nickel Oxide Catalysts over Various Supports to Produce Renewable Diesel Fuel. *Biomass Bioenergy* **2021,** *154*, 106248.
12. Giraldo, L.; Camargo, G.; Tirano, J.; Moreno-Pirajan, J., Synthesis of Fatty Alcohols from Oil Palm Using a Catalyst of Ni-Cu Supported onto Zeolite. *E-J. Chem.* **2010,** *7*, 1138-1147.
13. Ni, J.; Leng, W.; Mao, J.; Wang, J.; Lin, J.; Jiang, D.; Li, X., Tuning Electron Density of Metal Nickel by Support Defects in Ni/Zro_2 for Selective Hydrogenation of Fatty Acids to Alkanes and Alcohols. *Appl. Catal. B* **2019,** *253*, 170-178.
14. Cheah, K. W.; Taylor, M. J.; Osatiashtiani, A.; Beaumont, S. K.; Nowakowski, D. J.; Yusup, S.; Bridgwater, A. V.; Kyriakou, G., Monometallic and Bimetallic Catalysts Based on Pd, Cu and Ni for Hydrogen Transfer Deoxygenation of a Prototypical Fatty Acid to Diesel Range Hydrocarbons. *Catal. Today* **2020,** *355*, 882-892.
15. Zhang, J.; Zhao, C., Development of a Bimetallic Pd-Ni/Hzsm-5 Catalyst for the Tandem Limonene Dehydrogenation and Fatty Acid Deoxygenation to Alkanes and Arenes for Use as Biojet Fuel. *ACS Catal.* **2016,** *6*, 4512-4525.
16. D.J.Sajkowski; S.T.Oyama, Catalytic Hydrotreating by Molybdenum Carbide and Nitride Unsupported Mo_2n and Mo_2c/Al_2o_3 [1]. *Appl. Catal. A* **1996,** *134*, 339-349.
17. K.S. Weil; Kumta, P. N., Synthesis of Ternary Transition Metal Nitrides Using Chemically Complexed Precursors. *Mater. Sci. Eng. B* **1996,** *38* 109-117.
18. Schaidle, J. A.; Thompson, L. T., Fischer–Tropsch Synthesis over Early Transition Metal Carbides and Nitrides: Co Activation and Chain Growth. *J. Catal.* **2015,** *329*, 325-334.
19. R. Kojima; Aika, K., Molybdenum Nitride and Carbide Catalysts for Ammonia Synthesis. *Appl. Catal. A* **2001,** *219*, 141-147.
20. Xie, J.; Li, S.; Zhang, X.; Zhang, J.; Wang, R.; Zhang, H.; Pan, B.; Xie, Y., Atomically-Thin Molybdenum Nitride Nanosheets with Exposed Active Surface Sites for Efficient Hydrogen Evolution. *Chem. Sci.* **2014,** *5*, 4615-4620.
21. Ranhotra, G. S.; Bell, A. T.; Reimer, J. A., Catalysis over Molybdenum Carbides and Nitrides: Ii. Studies of Co Hydrogenation and C_2h_6 Hydrogenolysis. *J. Catal.* **1987,** *108*, 40-49.
22. Sankar, M.; Dimitratos, N.; Miedziak, P. J.; Wells, P. P.; Kiely, C. J.; Hutchings, G. J., Designing Bimetallic Catalysts for a Green and Sustainable Future. *Chem. Soc. Rev.* **2012,** *41*, 8099-8139.
23. Alonso, D. M.; Wettstein, S. G.; Dumesic, J. A., Bimetallic Catalysts for Upgrading of Biomass to Fuels and Chemicals. *Chem. Soc. Rev.* **2012,** *41*, 8075-8098.
24. Chen, W. F.; Sasaki, K.; Ma, C.; Frenkel, A. I.; Marinkovic, N.; Muckerman, J. T.; Zhu, Y.; Adzic, R. R., Hydrogen-Evolution Catalysts Based on Non-Noble Metal Nickel-Molybdenum Nitride Nanosheets. *Angew Chem Int Ed Engl* **2012,** *51*, 6131-5.
25. Chu, Y.; Wei, Z.; Yang, S.; Li, C.; Xin, Q.; Min, E., $Nimon_x/\Gamma\text{-}Al_2o_3$ Catalyst for Hdn of Pyridine. *Appl. Catal. A* **1999,** *176*, 17-26.
26. Egorova, M.; Prins, R., The Role of Ni and Co Promoters in the Simultaneous Hds of Dibenzothiophene and Hdn of Amines over $Mo/\Gamma\text{-}Al_2o_3$ Catalysts. *J. Catal.* **2006,** *241*, 162-172.

27. Lei, M.; Zhao, H.; Yang, H.; Song, B.; Cao, L.; Li, P.; Tang, W., Syntheses of Metal Nitrides, Metal Carbides and Rare-Earth Metal Dioxymonocarbodiimides from Metal Oxides and Dicyandiamide. *J. Alloys Compd.* **2008,** *460*, 130-137.
28. Buha, J.; Djerdj, I.; Antonietti, M.; Niederberger, M., Thermal Transformation of Metal Oxide Nanoparticles into Nanocrystalline Metal Nitrides Using Cyanamide and Urea as Nitrogen Source. *Chem. Mater.* **2007,** *19*, 3499-3505.
29. Sayo Soyama (nee Yokoi), M. I., Shigenobu Funahashi,* and Motoharu Tanaka, Variable-Temperature and -Pressure Multinuclear Magnetic Resonance Study of Solvent Exchange at the Tris(Ethylenediamine)Nickel(Ii) Ion in Ethylenediamine. *Inorg. Chem.* **1992,** *31*, 536-538.
30. Meng Chen, Y. X., Zhenyu Yao, Yitai Qian, Guien Zhou, A Novel Solvent-Directed Shape Control Technique for Preparation of Rod-Shaped Pbs Crystals. *Mater. Res. Bull.* **2002,** *37*, 247-253.
31. Y. Wang; Ling, , L.; Jiang, H., Selective Hydrogenation of Lignin to Produce Chemical Commodities by Using a Biochar Supported Ni–Mo_2c Catalyst Obtained from Biomass. *Green Chem.* **2016,** *18*, 4032–4041
32. Du, X.; Zhou, K.; Zhou, L.; Lei, X.; Yang, H.; Li, D.; Hu, C., Efficient Catalytic Conversion of Jatropha Oil to High Grade Biofuel on Ni-Mo_2c/Mcm-41 Catalysts with Tuned Surface Properties. *J. Energy Chem.* **2021,** *61*, 425-435.
33. Chen, Y.; Yu, J.; Jia, J.; Liu, F.; Zhang, Y.; Xiong, G.; Zhang, R.; Yang, R.; Sun, D.; Liu, H.; Zhou, W., Metallic Ni_3mo_3n Porous Microrods with Abundant Catalytic Sites as Efficient Electrocatalyst for Large Current Density and Superstability of Hydrogen Evolution Reaction and Water Splitting. *Appl. Catal. B* **2020,** *272*.
34. Böröczki, Á.; Dobos, G.; Josepovits, V. K.; Hárs, G., High Temperature Reactions between Molybdenum and Metal Halides. *Appl. Surf. Sci.* **2006,** *252*, 8309-8313.
35. Li, M.; Zhu, Y.; Wang, H.; Wang, C.; Pinna, N.; Lu, X., Ni Strongly Coupled with Mo_2c Encapsulated in Nitrogen-Doped Carbon Nanofibers as Robust Bifunctional Catalyst for Overall Water Splitting. *Adv. Energy Mater.* **2019,** *9*, 1803185.
36. Yan, H.; Xie, Y.; Jiao, Y.; Wu, A.; Tian, C.; Zhang, X.; Wang, L.; Fu, H., Holey Reduced Graphene Oxide Coupled with an Mo_2n-Mo_2c Heterojunction for Efficient Hydrogen Evolution. *Adv. Mater.* **2018,** *30*.
37. Du, X.; Li, N.; Zhang, X., Controlled Synthesis of Co_3o_4@$Nimoo_4$ Core-Shell Nanorod Arrays for Efficient Water Splitting. *Dalton Trans* **2018,** *47*, 12071-12074.
38. Wang, S.-G.; Lin, J.; Fan, C.-Y.; Li, Y.-F.; Zhang, J.-P.; Wu, X.-L.; Sun, H.-Z.; Deng, M.-X.; Su, Z.-M., Target Encapsulating $Nimoo_4$ Nanocrystals into 1d Carbon Nanofibers as Free-Standing Anode Material for Lithium-Ion Batteries with Enhanced Cycle Performance. *J. Alloys Compd.* **2020,** *830*.
39. Zhou, L.; Zeng, S.; Zheng, D.; Zeng, Y.; Wang, F.; Xu, W.; Liu, J.; Lu, X., $Nimoo_4$ Nanowires Supported on Ni/C Nanosheets as High-Performance Cathode for Stable Aqueous Rechargeable Nickel-Zinc Battery. *Chem. Eng. J.* **2020,** *400*.
40. Ohta, N., Scheuermann, W., Nakamoto, K., Matsuda, Y., Yamada, S., Murakami, Y., Resonance Raman Spectra of Tetrapyrrole Complexes of Oxomolybdenum(V). *Inorg. Chem.* **1979,** *18*, 457-460.
41. Xue, S.; Zhang, W.; Zhang, Q.; Du, J.; Cheng, H.-M.; Ren, W., Heterostructured Ni–Mo–N Nanoparticles Decorated on Reduced Graphene Oxide as Efficient and Robust Electrocatalyst for Hydrogen Evolution Reaction. *Carbon* **2020,** *165*, 122-128.
42. Chen, Y. Y.; Zhang, Y.; Zhang, X.; Tang, T.; Luo, H.; Niu, S.; Dai, Z. H.; Wan, L. J.; Hu, J. S., Self-Templated Fabrication of $Moni_4/Moo_{3-X}$ Nanorod Arrays with Dual Active Components for Highly Efficient Hydrogen Evolution. *Adv. Mater.* **2017,** *29*.
43. Persson, K., Materials Data on Ni3mo3n (Sg:227) by Materials Project. **2016**.

44. Jaf, Z. N.; Miran, H. A.; Jiang, Z.-T.; Altarawneh, M., Molybdenum Nitrides from Structures to Industrial Applications. *Rev. Chem. Eng.* **2021**.
45. Xing, S.; Liu, Y.; Liu, X.; Li, M.; Fu, J.; Liu, P.; Lv, P.; Wang, Z., Solvent-Free Hydrodeoxygenation of Bio-Lipids into Renewable Alkanes over Niw Bimetallic Catalyst under Mild Conditions. *Appl. Catal. B.* **2020,** *269*, 118718.
46. Miao, C.; Marin-Flores, O.; Davidson, S. D.; Li, T.; Dong, T.; Gao, D.; Wang, Y.; Garcia-Pérez, M.; Chen, S., Hydrothermal Catalytic Deoxygenation of Palmitic Acid over Nickel Catalyst. *Fuel* **2016,** *166*, 302-308.
47. Peng, B.; Zhao, C.; Kasakov, S.; Foraita, S.; Lercher, J. A., Manipulating Catalytic Pathways: Deoxygenation of Palmitic Acid on Multifunctional Catalysts. *Chemistry* **2013,** *19*, 4732-4741.
48. Yue, S.; Dong, L.; Liu, X.; Guo, Y.; Wang, Y., Hydrogenation of Palmitic Acid over Ni/Nb_2o_5-Sio_2 Catalyst: Synergetic Effect and Kinetic Study. *Ind Crops Prod* **2020,** *158*.
49. Sun, D.; Sato, S.; Ueda, W.; Primo, A.; Garcia, H.; Corma, A., Production of C_4 and C_5 Alcohols from Biomass-Derived Materials. *Green Chem.* **2016,** *18*, 2579-2597.
50. Voeste, T.; Buchold, H., Production of Fatty Alcohols from Fatty Acids. *J Am Oil Chem Soc* **1984,** *61*, 350-352.